Chapter

Exergoeconomic and Normalized Sensitivity Analysis of Plate Heat Exchangers: A Theoretical Framework with Application

Muhammad Ahmad Jamil, Talha S. Goraya, Haseeb Yaqoob, Kim Choon Ng, Muhammad Wakil Shahzad and Syed M. Zubair

Abstract

Heat exchangers are the mainstay of thermal systems and have been extensively used in desalination systems, heating, cooling units, power plants, and energy recovery systems. This chapter demonstrates a robust theoretical framework for heat exchangers investigation based on two advanced tools, i.e., exergoeconomic analysis and Normalized Sensitivity Analysis. The former is applied as a mutual application of economic and thermodynamic analyses, which is much more impactful than the conventional thermodynamic and economic analyses. This is because it allows the investigation of combinatory effects of thermodynamic and fiscal parameters which are not achieved with the conventional methods. Similarly, the Normalized Sensitivity Analysis allows a one-on-one comparison of the sensitivity of output parameters to the input parameters with entirely different magnitudes on a common platform. This rationale comparison is obtained by normalizing the sensitivity coefficients by their nominal values, which is not possible with the conventional sensitivity analyses. An experimentally validated example of a plate heat exchanger is used to demonstrate the application of the proposed framework from a desalination system.

Keywords: exergoeconomic analysis, normalized sensitivity analysis, heat exchangers, theoretical framework

1. Introduction

Heat exchangers are an essential component of thermal systems and increase system efficiency by recovering heat from the waste streams [1]. Heat exchangers play a vital role in several applications i.e., waste heat recovery, thermal desalination units, power plants, air conditioning, refrigeration, manufacturing industry, food, chemical, and process industries, etc. The water purification industry that fulfills ~40% of water demand worldwide is based on thermal-based desalination systems [2]. These systems include mechanical/thermal vapor compression (TVC/MVC) systems, adsorption systems, multi-effect desalination (MED), and

multistage flash (MSF) [3]. These systems are mostly used due to their high operational reliability, ability to use low-grade energy, low pre-and-post treatment requirement, and capability to treat harsh feeds [4]. Thermal-based desalination systems operate at high brine temperature, and several pieces of research have been carried to improve their thermal and economic performance [5]. One of the major improvements in this regard is energy recovery by using a preheater. The additional component recovers heat from the waste stream i.e., brine, and preheat the intake stream which reduces thermal losses, decreases the evaporator loads, area, and investment [6].

Plate heat exchangers (PHXs) are widely used for heat recovery in thermal-based desalination units as a preheater. The plate heat exchanger offers many benefits including narrow temperature control ($\Delta T \leq 5°C$), easy maintenance and cleaning, margin to accommodate different loads, and high operational reliability [7]. Furthermore, it is significant to indicate that PHXs as preheaters have rarely been examined in thermal-based desalination units from an optimized cost design and analysis viewpoint [8]. Rather, the conducted studies either are restricted to preliminary sizing [9] or heat exchanger design is missing [10]. In conventional studies, the heat transfer area is calculated by the temperature-based heat transfer coefficient correlation offered by Dessouky et al. [11]. However, this method gives a fast estimation of heat transfer area, but the accuracy and reliability of the method are doubtful. This is because, in the heat exchangers, the heat transfer coefficient is the function of different parameters such as pressure, temperature, thermophysical properties, flow characteristics, and geometric parameter [12].

For example, in many previous studies, the plate chevron angle (β) is reported as the most influential geometrical variable of PHXs from the thermal–hydraulic performance viewpoint [13]. Likewise, the heat duty, thermophysical properties, and flow rates also have a remarkable impact on PHXs performance [14]. Some recent optimization studies highlighted the importance of various other process and geometric variables that significantly affect the PHXs performance [15]. For instance, the most critical and influential parameters that have been reported are dimensions of chevron corrugation, number of passes, number of plates, type of plate, and channel flow type (parallel, counter, mixed, etc.) [16].

As it appears from the above literature review that there is a requirement for a laborious optimum cost design and detailed investigation of the preheaters for the thermal-based water treatment systems. In this regard, Jamil et al. [17] moderately addressed the issues and conducted a detailed thermal–hydraulic analysis but have deficiencies in the economic analysis viewpoint. This book chapter is focused on the combinatory effect of thermal, hydraulic, and economic analysis. Furthermore, normalized sensitivity analysis and exergoeconomic analysis are also conducted. This chapter will discuss the sections as follow (a) exergoeconomic analysis methodology, (b) normalized sensitivity analysis methodology, (c) experimentally validation of the numerical model, (d) normalized sensitivity analysis in term of NSC and RC, and (e) exergoeconomic analysis. The normalized sensitivity and exergoeconomic analysis are conducted for a preheater (PHX) of a single evaporator based MVC desalination system as a case study.

2. Exergoeconomic analysis methodology

2.1 Heat exchanger configuration

Figure 1 represents the schematic diagram of the current considered system. The system includes PHXs and two centrifugal pumps to maintain the desire flow

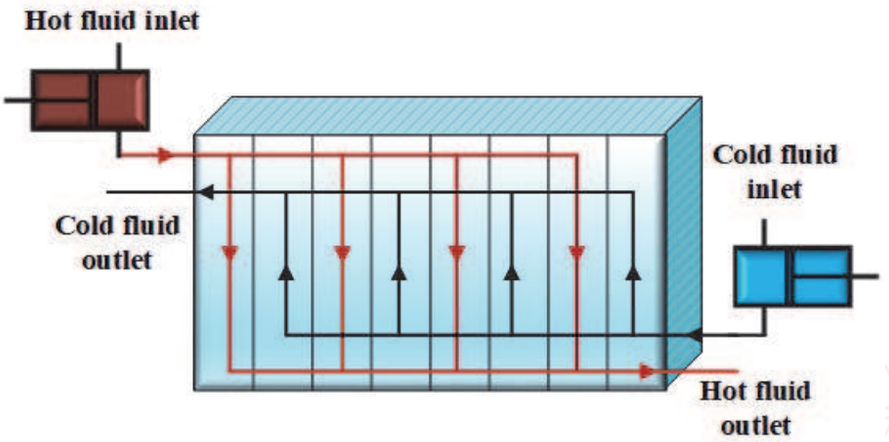

Figure 1.
Plate heat exchanger configuration for current case study.

Parameter		Value
Mass flow rate	Seawater, $\dot{m}_{SW}$ (kg/s)	13
	Brine, $\dot{m}_B$ (kg/s)	13
Temperature of seawater	Inlet, $T_{SW,i}$ (°C)	21
	Outlet, $T_{SW,o}$ (°C)	57
Temperature of Brine	Inlet, $T_{B,i}$ (°C)	63
	Outlet, $T_{B,o}$ (°C)	23
Salinity	Sea water, S_{SW} (g/kg)	40
	Brine, S_B (g/kg)	80

Table 1.
Input operation variables for the current case study [18].

rates and overcome the pressure losses. The PHXs are used as a preheater in single evaporator based MVC water treatment system [18] to preheat the intake seawater using hot brine water. The operational variables i.e., mass flow rates, salinity, the temperature of hot and cold streams are extracted from our recent studies, as mentioned in **Table 1** [18].

2.2 Thermal–hydraulic analysis model

The thermo hydraulic design of the PHXs presented previous study [17] is used for the calculation of different parameters such as flow rates, temperature, area, pressure drop, heat duty, local and global heat transfer coefficient, etc. In the thermal investigation, Nusselt number (Nu) is one of the most important parameters and can be calculated using a correlation (Eq. (1)) which is primarily dependent on the Reynold number (Re) and Prandtl number (Pr) [19].

$$Nu = C_h \,\mathrm{Re}^{n}\ \ \mathrm{Pr}^{0.333}\left(\frac{\mu}{\mu_w}\right)^{0.17} \tag{1}$$

Where the value of C_h and n with different Reynold number and Chevron angle is given in [19]. The governing equations for the calculation of a detailed thermal

Variables	Units	Formula
Reynold number	—	$\mathrm{Re} = \nu_{chl} \times D_{hyd}/\mu$
Mass velocity per channel	kg/m^2s	$\nu_{chl} = \dot{m}/N_{cpp} \times A_{chl}$
Number of channels per pass	—	$N_{cpp} = N_{tb}–1/2 \times N_P$
Single-channel flow area	m^2	$A_{chl} = L_w \times B$
Mean channel flow gap	—	$B=PP–t_{plate}$
Plate pitch	m	$PP = L_c/N_{tb}$
Hydraulic diameter	m	$D_{hyd} = 2\times B/EF$
Projected plate area	m^2	$A_p = (L_v–D_p) \times L_w$
Enlargement factor	—	$A_{sp} = EF \times A_p$
Effective area	m^2	$A = A_{sp} \times N_e$
Effective number of plates	—	$N_e = N_{tb}–2$
Local heat transfer coefficient	kW/m^2K	$h = Nu\times k/D_{hyd}$
Overall clean heat transfer coefficient	kW/m^2K	$\frac{1}{U_{cl}} = \frac{1}{h_c} + \frac{t_{plate}}{k_{plate}} + \frac{1}{h_h}$
Overall heat transfer coefficient	kW/m^2K	$\frac{1}{U_{fo}} = \frac{1}{U_{cl}} + R_{fo,\mathrm{total}}$
Factor of Cleanliness	—	$FOC = U_{fo}/U_{cl}$
Over surface design	%	$OSD = (U_c + R_{fo,\mathrm{total}})\times 100$
Heat duty	kW	$\dot{Q} = A_e \times U \times \Delta T_{LMTD}$

Table 2.
Thermal design equations of PHXs [19].

model are summarized in **Table 2**. While the implementation and selection of correlation are discussed and summarized in [17].

The hydraulic analysis includes the investigation of pumping power and total pressure drop, which is dependent on various pressure losses i.e., ports losses, manifolds losses, and channels losses as shown below [13, 19].

$$\Delta P_{tot} = \Delta P_{chl} + \Delta P_{po} + \Delta P_{man} \tag{2}$$

The pumping power can be calculated as.

$$P_{power} = \frac{\dot{m}\,\Delta P_{tot}}{\eta_p \rho} \tag{3}$$

The governing equation of the remaining hydraulic model is summarized in **Table 3**.

2.3 Exergy and exergoeconomic analysis

For the heat exchanger analysis, exergy analysis is a significant and reliable technique because it includes the exergy destruction calculation [20]. The exergy analysis measures overall performance and concurrently responsible for the changes in temperature and pressure. The exergy destruction calculations estimate the performance index of the analysis [21]. For the analysis, the flow exergy is determined at boundaries (inlet and outlet) of pumps and heat exchangers based on their operational

Variables	Units	Formula
Pressure drops in the channel	kPa	$\Delta P_{chl} = 4 \times ff \times \frac{L_e \times N_p}{D_{hyd}} \times \frac{\nu_{chl}^2}{2\times\rho} \times \left(\frac{\mu}{\mu_w}\right)^{-0.17}$
Pressure drops in ports	kPa	$\Delta P_{po} = 1.4 \times N_P \times \frac{\nu_p^2}{2\times\rho}$
Portside mass velocity	kg/m^{2}s	$\nu_p = \frac{\dot{m}}{\pi \times \left(\frac{D_p^2}{4}\right)}$
Pressure drop in manifold	kPa	$\Delta P_{man} = 1.5 \times \left(\frac{V^2}{2\times v_s}\right)$
Friction factor	—	$ff = \frac{K_P}{\mathrm{Re}^m}$

Table 3.
Hydraulic design equations of PHXs [13, 19].

parameters such as mass flow rates, temperature, pressure, and salinity, as given in Eq. (4). After that, Eq. (6) is solved for all the components to get the exergy destruction. In the present study, the seawater database is used for the calculation of specific flow exergy $\overline{EX}$ and thermophysical properties [22].

$$\overline{EX} = \left[\left(h' - h_0'\right) - T_0(s - s_0)\right] + \overline{EX}_{che} \tag{4}$$

$$\dot{E} = \dot{m} \times \overline{EX} \tag{5}$$

$$\dot{E}_D = \dot{E}_i - \dot{E}_o \tag{6}$$

For the heat exchanger, the economic investigation is depending on the capital/purchasing investment (CI) and operational/running cost (OC) [23]. However, for the large component of the system, such as power plants and desalination units, the product cost is more important than purely capital investment and operational cost [24] because, in these systems, the performance of HX is primarily dependent upon the plant process variables. Therefore, the HX is analyzed and designed to meet the plant requirement [6, 18] instead of optimum HX performance.

The total cost of the heat exchanger is the sum of the capital investment (CI) and operational cost (OC) as given below [25].

$$C_{tot} = CI + OC \tag{7}$$

The capital investment (CI) is the initial amount required to purchase equipment based on time and location of analysis. The finest method to calculate the capital investment to use the experimental correlations purposed by researchers and vendors after extensive study and survey. In the current study, the capital investment of the pump and heat exchanger is calculated using the most common and reliable correlations presented in [26, 27].

The capital investment correlations used for the heat exchanger are generally dependent upon the heat transfer area as [28].

$$CI_{PHX}^{\$} = 1000 \times \left(12.86 + A^{0.8}\right) \times IF \tag{8}$$

After that, an installation factor (IF) range from 1.5 to 2.0 is used to predict accurately the monetary of the equipment at the utility. In contrast, the capital investment of the pump is calculated as [27].

$$CI_P^{\$} = 13.92 \times \ \dot{m} \times \ \Delta P^{0.55} \times \left(\eta_p / \left(1 - \eta_p\right)\right)^{1.05} \tag{9}$$

A detailed discussion regarding the capital investment correlation is given in the reference study [29]. Furthermore, the constant in the correlation is varying with material selection and the applicability range. The empirical correlations are developed a long time ago based on the fiscal policy of that era. Therefore, all the above correlations need a slight correction to accurately estimate the capital investment in the current time. In this aspect, the cost index factor (C_{index}) is commonly used. The C_{index} is calculated by using Eq. (10) in which the chemical engineering plant cost index (CEPCI) is used for the original year and the present year as given as [30, 31].

$$C_{index} = \frac{CEPCI_{current}}{CEPCI_{reference}} \tag{10}$$

$$CI^{\$}_{current} = C_{index} \times CI^{\$}_{reference} \tag{11}$$

In the present analysis, the C_{index} 1.7 is used based on their CEPCI 390 [32] and CEPCI 650 for the year of 1990 and 2020 [33] respectively. However, the importance of the Cost index is analyzed from different ranges in the result and discussion section. Likewise, the operation cost (OC) is calculated using Eq. (12). The OC is primarily dependent on the pumping power, P_{Power} (kW), yearly current cost, C_y ($/y), the unit cost of electricity, C_{ele} ($/kWh), inflation rate, i (%), operating hours, Φ (h/y), and component life, n_y (year).

$$OC = \sum_{j=1}^{n_y} \frac{C_y}{(1+i)^{\ j}} \tag{12}$$

$$C_o = P_{power} \times C_{ele} \times \Phi \tag{13}$$

$$P_{power} = \frac{1}{\eta_p}\left(\frac{\dot{m}_{SW} \times \Delta P_{SW}}{\rho_{SW}} + \frac{\dot{m}_B \times \Delta P_B}{\rho_B}\right) \tag{14}$$

Whereas, the values operating hours Φ = 7000 h/y, component life n_y = 10 years, unit cost of electricity C_{ele} = 0.09 ($/KWh) and efficiency of pump η_p = 78% [25] are used in current analysis.

The output cost of the hot stream can be calculated by implementing the general cost approach [18]. For this purpose, the pre-calculated capital investment is converted into the yearly capital investment rate $\dot{\Gamma}\,(\$/y)$ by using the capital recovery factor (r) [6].

$$r = \frac{i \times (1+i)^{n_y}}{(1+i)^{n_y} - 1} \tag{15}$$

$$\dot{\Gamma} = r \times CI \tag{16}$$

After that, the annual rate is transferred into the fixed cost rate $\varsigma\ (\$/s)$ through the plant availability factor (Φ).

$$\varsigma = \frac{\dot{\Gamma}}{3600 \times \Phi} \tag{17}$$

After determining the cost flow rate, the cost balance takes the form mentioned below.

$$C_o = \Sigma C_i + \varsigma \tag{18}$$

Whereas the ς is the component cost rate, C_i is the cost of the inlet stream and C_o is the product cost of the outlet stream. The cost balance (refers to Eq. (18)) is re-arranged for the cost balance of the heat exchanger and pump as.

$$C_o = C_i + C_{ele} \times \dot{W}_P + \varsigma_P \tag{19}$$

$$C_{c,o} = C_{c,i} + C_{h,i} - C_{h,o} + \varsigma_{PHX} \tag{20}$$

The cost of the inlet stream is varying from case to case. For the current case study, the inlet cost of the seawater is chosen from the study. It is important to mention that the equipment with various outputs such as RO trains, HXs, flashing stages, evaporation effects, etc.,) need an additional equation for the result. For instance, for the component with "k" outputs, a "k-1" number of additional equations are required. The cost balance of the plate heat exchanger (PHXs) can be solved by using the supplementary equation (Eq. (21)). The equivalency of the average inlet cot and outlet cost of streams depends on these additional Equations [29].

$$\frac{C_{B,i}}{E_{B,i}} - \frac{C_{B,o}}{E_{B,o}} = 0 \tag{21}$$

3. Normalized sensitivity analysis methodology

The sensitivity analysis is an important tool to examine the behavior of output performance parameters against the different input variables [34]. Sensitivity analysis is a significant tool to identify the influential and critical performance parameters and highlights the design improvements for future research. For this purpose, calculus-based (partial derivative-based) sensitivity analysis is one of the most trustworthy and widely used methods. In this approach, all the independent parameters sum up their nominal values and uncertainty as given below [35].

$$X = \overline{X} \pm \widehat{U}_X \tag{22}$$

where $\overline{X}$ and $\pm\widehat{U}_X$ represents the nominal value and the uncertainty about the nominal value, respectively. The uncertainty in the output performance parameter Y(X) because of the uncertainty of variable X is given below [35].

$$\widehat{U}_Y = \frac{dY}{dX}\widehat{U}_X \tag{23}$$

The total uncertainty for the multi-variable function is given as.

$$\widehat{U}_Y = \left[\sum_{j=1}^{N}\left(\frac{\partial Y}{\partial X_j}\widehat{U}_{X_j}\right)^2\right]^{1/2} \tag{24}$$

The partial derivative parameter in the total uncertainty equation denotes the sensitivity coefficient (SC) of the selected output parameter. These SC are converted into modified forms knowns as the Normalized Sensitivity Coefficient (NSC) by regulating the uncertainty in the outlet variable Y and input variable X by their corresponding nominal value ($\overline{X}$). The NSC provides a comparison of all the input variables with significantly different magnitude based on their critical

impact on the desired performance parameter [36]. The NSC can be written mathematically as [35].

$$\frac{\widehat{U}_Y}{\overline{Y}} = \left[\sum_{j=1}^{N} \overbrace{\left(\frac{\partial Y}{\partial X_j}\frac{\overline{X}_j}{\overline{Y}}\right)^2}^{NSC} \overbrace{\left(\frac{\widehat{U}_{Xj}}{\overline{X}_j}\right)^2}^{N\widehat{U}_{Xj}}\right]^{1/2} \tag{25}$$

Where NU denotes the normalized uncertainty, and NSC denotes the normalized sensitivity coefficient. Thus, the Eq. (25) can be written for the selected output performance parameters in term of NSC as follow.

$$\frac{\widehat{U}_{h_c}}{\overline{h}_c} = \left[\begin{array}{l}\left(\frac{\partial h_c}{\partial \dot{m}_c}\frac{\overline{\dot{m}}_c}{\overline{h}_c}\right)^2\left(\frac{\widehat{U}_{\dot{m}_c}}{\overline{\dot{m}}_c}\right)^2 + \left(\frac{\partial h_c}{\partial \dot{m}_h}\frac{\overline{\dot{m}}_h}{\overline{h}_c}\right)^2\left(\frac{\widehat{U}_{\dot{m}_h}}{\overline{\dot{m}}_h}\right)^2 + \left(\frac{\partial h_c}{\partial T_{c,i}}\frac{\overline{T}_{c,i}}{\overline{h}_c}\right)^2\left(\frac{\widehat{U}_{T_{c,i}}}{\overline{T}_{c,i}}\right)^2 \\ +\left(\frac{\partial h_c}{\partial T_{h,\mathrm{i}}}\frac{\overline{T}_{h,\mathrm{i}}}{\overline{h}_c}\right)^2\left(\frac{\widehat{U}_{T_{h,\mathrm{i}}}}{\overline{T}_{h,\mathrm{i}}}\right)^2 + \left(\frac{\partial h_c}{\partial S_c}\frac{\overline{S}_c}{\overline{h}_c}\right)^2\left(\frac{\widehat{U}_{S_c}}{\overline{S}_c}\right)^2 + \left(\frac{\partial h_c}{\partial S_h}\frac{\overline{S}_h}{\overline{h}_c}\right)^2\left(\frac{\widehat{U}_{S_h}}{\overline{S}_h}\right)^2\end{array}\right]^{1/2} \tag{26}$$

$$\frac{\widehat{U}_{\Delta P_c}}{\overline{\Delta P_c}} = \left[\begin{array}{l}\left(\frac{\partial \Delta P_c}{\partial \dot{m}_c}\frac{\overline{\dot{m}}_c}{\overline{\Delta P_c}}\right)^2\left(\frac{\widehat{U}_{\dot{m}_c}}{\overline{\dot{m}}_c}\right)^2 + \left(\frac{\partial \Delta P_c}{\partial \dot{m}_h}\frac{\overline{\dot{m}}_h}{\overline{\Delta P_c}}\right)^2\left(\frac{\widehat{U}_{\dot{m}_h}}{\overline{\dot{m}}_h}\right)^2 + \left(\frac{\partial \Delta P_c}{\partial T_{c,i}}\frac{\overline{T}_{c,i}}{\overline{\Delta P_c}}\right)^2\left(\frac{\widehat{U}_{T_{c,i}}}{\overline{T}_{c,i}}\right)^2 \\ +\left(\frac{\partial \Delta P_c}{\partial T_{h,i}}\frac{\overline{T}_{h,i}}{\overline{\Delta P_c}}\right)^2\left(\frac{\widehat{U}_{T_{h,i}}}{\overline{T}_{h,i}}\right)^2 + \left(\frac{\partial \Delta P_c}{\partial S_c}\frac{\overline{S}_c}{\overline{\Delta P_c}}\right)^2\left(\frac{\widehat{U}_{S_c}}{\overline{S}_c}\right)^2 + \left(\frac{\partial \Delta P_c}{\partial S_h}\frac{\overline{S}_h}{\overline{\Delta P_c}}\right)^2\left(\frac{\widehat{U}_{S_h}}{\overline{S}_h}\right)^2\end{array}\right]^{1/2} \tag{27}$$

$$\frac{\widehat{U}_{OC}}{\overline{OC}} = \left[\begin{array}{l}\left(\frac{\partial OC}{\partial \dot{m}_c}\frac{\overline{\dot{m}}_c}{\overline{OC}}\right)^2\left(\frac{\widehat{U}_{\dot{m}_c}}{\overline{\dot{m}}_c}\right)^2 + \left(\frac{\partial OC}{\partial \dot{m}_h}\frac{\overline{\dot{m}}_h}{\overline{OC}}\right)^2\left(\frac{\widehat{U}_{\dot{m}_h}}{\overline{\dot{m}}_h}\right)^2 + \left(\frac{\partial OC}{\partial S_c}\frac{\overline{S}_c}{\overline{OC}}\right)^2\left(\frac{\widehat{U}_{S_c}}{\overline{S}_c}\right)^2 \\ +\left(\frac{\partial OC}{\partial \eta_p}\frac{\overline{\eta}_p}{\overline{OC}}\right)^2\left(\frac{\widehat{U}_{\eta_p}}{\overline{\eta}_p}\right)^2 + \left(\frac{\partial OC}{\partial i}\frac{\bar{i}}{\overline{OC}}\right)^2\left(\frac{\widehat{U}_i}{\bar{i}}\right)^2 + \left(\frac{\partial OC}{\partial C_{ele}}\frac{\overline{C}_{ele}}{\overline{OC}}\right)^2\left(\frac{\widehat{U}_{C_{ele}}}{\overline{C}_{ele}}\right)^2\end{array}\right]^{1/2} \tag{28}$$

$$\frac{\widehat{U}_{C_{c,o}}}{\overline{C}_{c,o}} = \left[\begin{array}{l}\left(\frac{\partial C_{c,o}}{\partial \dot{m}_c}\frac{\overline{\dot{m}}_c}{\overline{C}_{c,o}}\right)^2\left(\frac{\widehat{U}_{\dot{m}_c}}{\overline{\dot{m}}_c}\right)^2 + \left(\frac{\partial C_{c,o}}{\partial \dot{m}_h}\frac{\overline{\dot{m}}_h}{\overline{C}_{c,o}}\right)^2\left(\frac{\widehat{U}_{\dot{m}_h}}{\overline{\dot{m}}_h}\right)^2 + \left(\frac{\partial C_{c,o}}{\partial T_{h,i}}\frac{\overline{T}_{h,i}}{\overline{C}_{c,o}}\right)^2\left(\frac{\widehat{U}_{T_{c,i}}}{\overline{T}_{c,i}}\right)^2 \\ +\left(\frac{\partial C_{c,o}}{\partial S_c}\frac{\overline{S}_c}{\overline{C}_{c,o}}\right)^2\left(\frac{\widehat{U}_{S_c}}{\overline{S}_c}\right)^2 + \left(\frac{\partial C_{c,o}}{\partial \eta_p}\frac{\overline{\eta}_p}{\overline{C}_{c,o}}\right)^2\left(\frac{\widehat{U}_{\eta_p}}{\overline{\eta}_p}\right)^2 + \left(\frac{\partial C_{c,o}}{\partial i}\frac{\bar{i}}{\overline{C}_{c,o}}\right)^2\left(\frac{\widehat{U}_i}{\bar{i}}\right)^2 \\ +\left(\frac{\partial C_{c,o}}{\partial C_{ele}}\frac{\overline{C}_{ele}}{\overline{C}_{c,o}}\right)^2\left(\frac{\widehat{U}_{C_{ele}}}{\overline{C}_{ele}}\right)^2 + \left(\frac{\partial C_{c,o}}{\partial C_{index}}\frac{\overline{C}_{index}}{\overline{C}_{c,o}}\right)^2\left(\frac{\widehat{U}_{C_{index}}}{\overline{C}_{index}}\right)^2\end{array}\right]^{1/2} \tag{29}$$

Where in the above equations the parameters correspond to the following: $\widehat{U}_{h_c}$: uncertainty in cold side heat transfer coefficient, $\widehat{U}_{\Delta P_c}$: uncertainty in cold side pressure drop, $\overline{\Delta P_c}$: nominal value of the cold side pressure drop, $\widehat{U}_{OC}$: uncertainty in operating cost, $\overline{OC}$: nominal value of the operating cost, $\widehat{U}_{C_{c,o}}$: uncertainty in the cold fluid outlet stream cost, $\overline{C_{c,o}}$: nominal value of the cold fluid outlet stream cost, $\overline{h}_c$: nominal value of cold side heat transfer coefficient, $\widehat{U}_{\dot{m}_c}$: uncertainty in cold side flow rate, $\overline{\dot{m}}_c$: nominal value of cold side flow rate, $\overline{\dot{m}}_h$: nominal value of hot side flow rate, $\widehat{U}_{\dot{m}_h}$: uncertainty in hot side flow rate, $\overline{T}_{c,i}$: nominal value of cold fluid inlet temperature, $\widehat{U}_{T_{c,i}}$: uncertainty in cold side inlet temperature, $\overline{T}_{h,i}$: nominal value of hot fluid inlet temperature, $\widehat{U}_{T_{h,i}}$: uncertainty in hot side inlet temperature, $\overline{S}_c$: nominal value of the cold fluid salinity, $\widehat{U}_{S_c}$: uncertainty in the cold fluid salinity,

$\overline{S}_h$: nominal value of the hot fluid salinity, $\widehat{U}_{S_h}$: perturbation in the hot fluid salinity, $\widehat{U}_{\eta_p}$: uncertainty in the pump efficiency value, $\overline{\eta}_p$: nominal value of the pump efficiency, $\widehat{U}_i$: uncertainty in the interest rate, $\overline{i}$: nominal value of the interest rate, $\widehat{U}_{C_{ele}}$: uncertainty in the the electricity cost, $\overline{C}_{ele}$: nominal value of the electricity cost, $\widehat{U}_{C_{index}}$: uncertainty in the cost index factor, $\overline{C}_{index}$: nominal value of the cost index factor.

The relative contribution (RC) is an important parameter in a normalized sensitivity analysis that is used to identify the variable with dominant uncertainty contribution through combining the sensitivity coefficient (SC) with the actual uncertainty. It can calculate as [35].

$$RC = \frac{\left(\frac{\partial Y}{\partial X_j}\widehat{U}_{Xj}\right)^2}{\widehat{U}_Y^2} \tag{30}$$

The working of normalized sensitivity analysis is quite simple. **Figure 2** represents the working methodology of normalized sensitivity analysis. At the start, all the input variables and output performance variables are selected. After that, the uncertainty/perturbation is selected that is generally 1% of the nominal value. In the next step, the partial derivative is taken for each output variable against the various input parameters. After the partial derivate of each variable, the sensitivity coefficient is calculated by using Eq. (23) for all the output variables. In the next step, the total uncertainty and normalized sensitivity of the output variable are calculated by using Eqs. (24) and (25). In the end, derived all the most significant, critical, and dominant input variables in terms of NSC and RC by using Eqs. (26)–(30).

4. Experimental validation of the numerical model

The normalized sensitivity and exergoeconomic techniques are applied on a preheater (plate heat exchanger) of SEE-MVC based-thermal desalination system for which the input data is already summarized in **Table 1**.

For the analysis purpose, a numerical model is developed on Engineering Equation Solver (EES) based using the governing equation mentioned above for which the solution flow chart is presented in **Figure 3**. After that, the developed numerical code is validated with the laboratory/experimental readings from a small-scale PHX as illustrated in **Figure 4**. The specifications of the laboratory scale PHX are mentioned in our previous study [17]. Then, the experiment is carried out for two different operating conditions. For each scenario, the experimental setup is operated for 35 minutes, and readings are saved through a data acquisition system (edibon SCADA) when the system becomes stable. After that, the experimental data are compared with numerical data, as shown in **Figure 5**. The numerical and experimental readings have very close values, which shows the accuracy of the numerical data.

4.1 Normalized sensitivity analysis in terms of NSC and RC

The analysis is carried to identify the most critical and crucial input variable that affects the selected output performance parameters. The desired output performance parameters are local cold side heat transfer coefficient, cold side pressure drop, operational cost, and product cost of the cold stream. **Figure 6** presents the

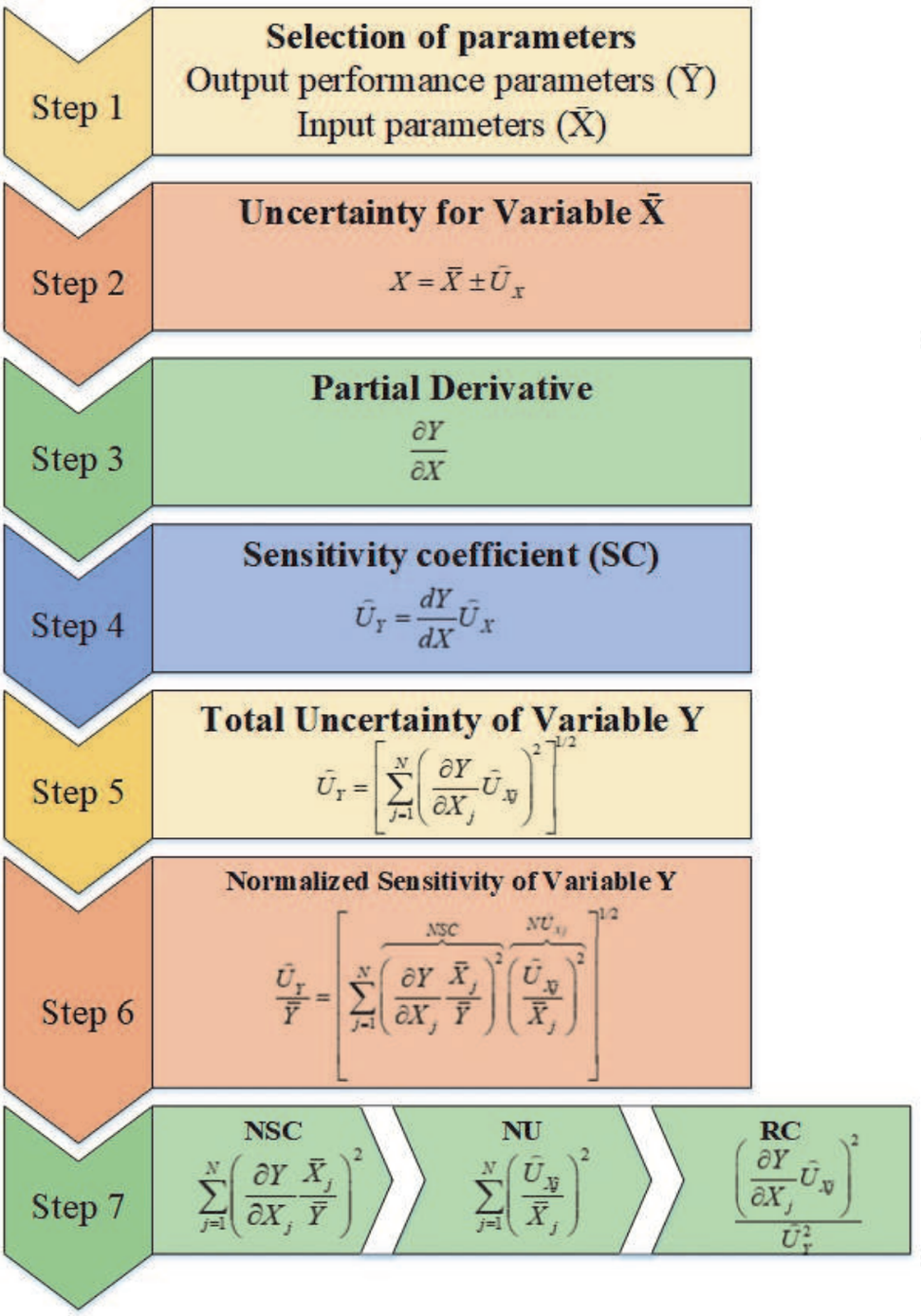

Figure 2.
Working flow chart of normalized sensitivity analysis.

sensitivity analysis results from Normalized Sensitivity Coefficient (NSC) and Relative Contribution (RC). From **Figure 6a**, it can be concluded that for the local heat transfer coefficient, the most crucial variables in terms of NSC are in the following order: cold side mass flow rate $\dot{m}_c$ > inlet temperature of cold side $T_{c,i}$ > salinity of cold side S_c while the RC is highest for cold side mas flow rate $\dot{m}_c$ with ~88% dominancy followed by inlet temperature of cold side with ~11.7% and salinity with ~0.05%. Likewise, for the cold side pressure drop ΔP_c, the most significant variable is $\dot{m}_c$ followed by $T_{c,i}$ while their corresponding RC is 99.6% and 0.4%, respectively as shown in **Figure 6b**. Similarly, from the monetary point of view, the operation cost (OC) highlights that the most influential input variables are $\dot{m}_c$ followed by $\dot{m}_h$, C_{ele}, i, and η_p. The RC is dominated by C_{ele}, with ~86.2% followed by i with ~8.94%,

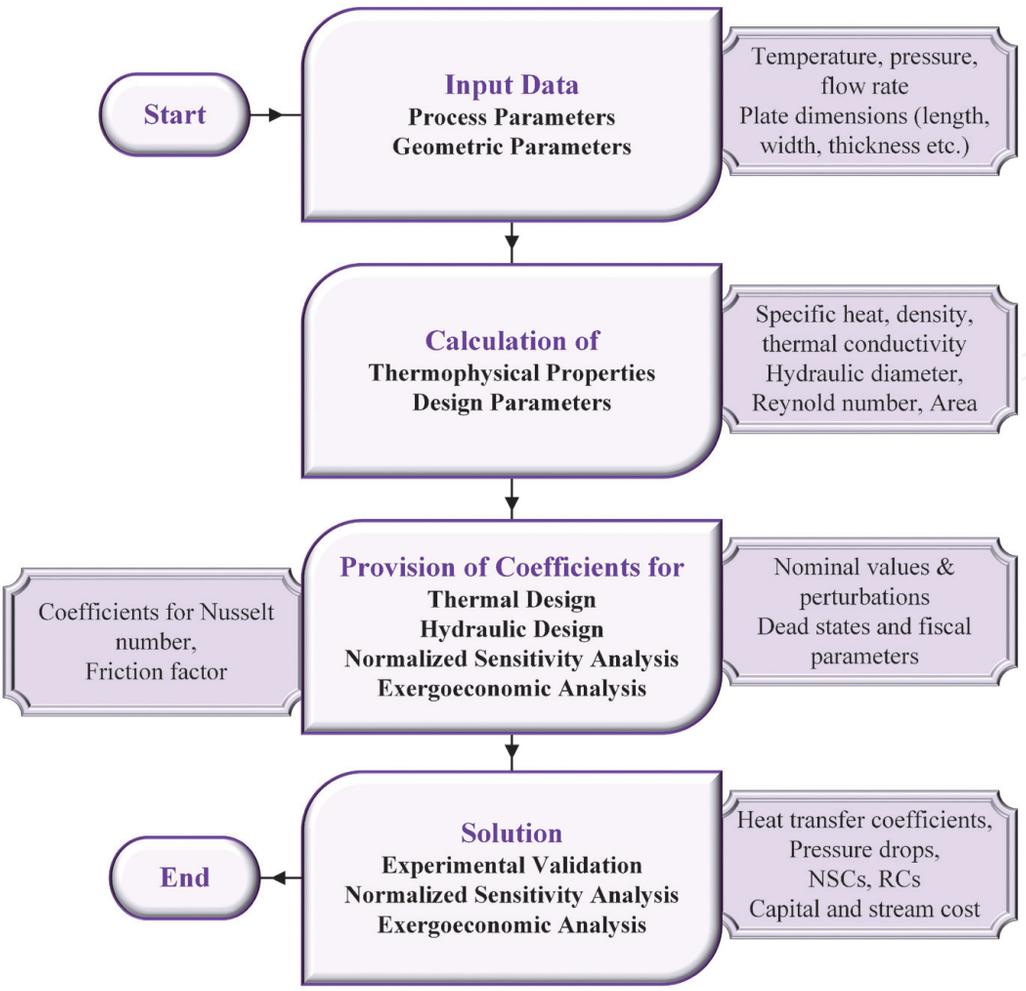

Figure 3.
Solution flow chart for numerical analysis.

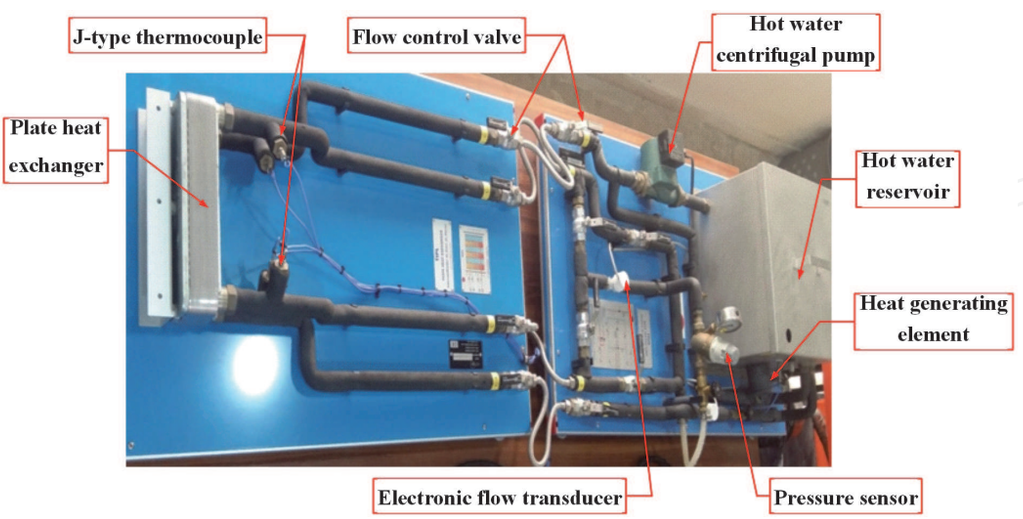

Figure 4.
Experimental test setup.

$\dot{m}_c$ with ~1.88%, $\dot{m}_h$ with ~1.84%, and η_p with ~ 1.15% as illustrated in **Figure 6c**. **Figure 6d** highlights the results of the product cost of the cold stream $C_{c,o}$. The most critical variables in terms of NSC are cost index C_{index} followed by $i, T_{h,i}, \eta_p, \dot{m}_c, \dot{m}_h$ and C_{ele} while the RC is maximum for the inflation rate i with ~95.5%.

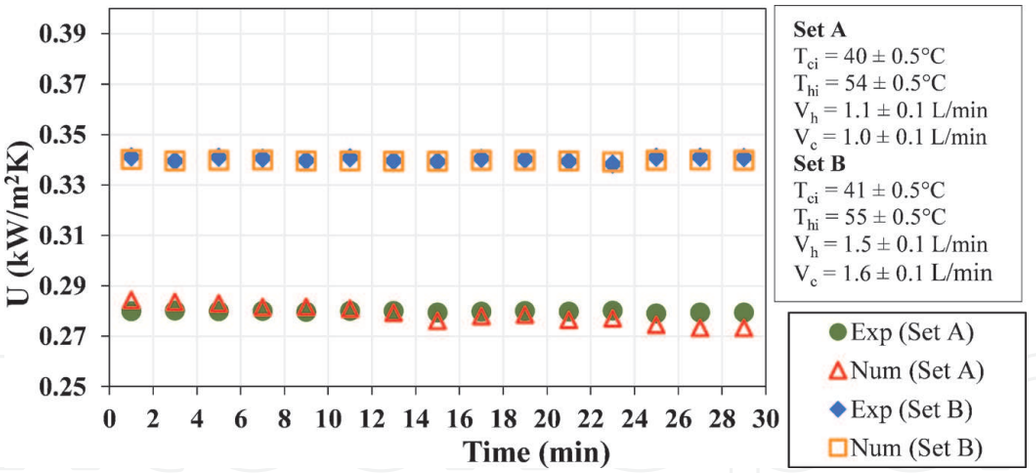

Figure 5.
Model validation with experimental data [17].

Overall, it was observed that the exergoeconomic analysis of PHX is affected by both fascial and process variables. Therefore, fascial parameters must consider equally while designing/analyzing PHX.

4.2 Exergoeconomic analysis

The thermal–hydraulic performance of PHXs is significantly affected by plate chevron angle (β) and mass flow rate [17]. The heat transfer coefficient and pressure drop of the cold stream are increased by varying the Reynold number (Re). However, the rise in heat transfer coefficient is desirable, but the rise in pressure drop is not favorable from a monetary viewpoint. Therefore, the comprehensive parameters (h/ΔP) are calculated to provide a reasonable estimate of heat transfer per unit pressure drop.

From **Figure 7**, the comprehensive performance parameters are declined with the increasing Reynold number. This is because with increasing Reynold number, the pressure drop increased at a higher-order rise compared to the heat transfer coefficient. Furthermore, the analysis is carried out for different chevron angles (β). It can be observed, the h/ΔP is highest for β = 60° followed by β = 50° > 45° > 30°. This is because the pressure drop faces less resistance at a high chevron angle. Meanwhile, from the economic viewpoint, the operation cost (OC) increased as the Reynold number increased. This is because, at the high6Reynold number, the pressure drop is increased which increased the energy consumption and ultimately the pumping power. The operational cost is highest for the chevron angle β = 30° and lowest for chevron angle β = 60° due to low-pressure loss.

Similarly, the product cost of the cold stream $C_{c,o}$ is also increased by varying Reynold number due to increased unit cost of electricity because, at a high Reynold number (flow rate), the pumping power is increased with consumes more energy compared to low-pressure drop. Furthermore, the outlet cost is highest for chevron angle β = 30° followed by β = 45° > 50° > 60°. This is because at a high chevron angle the pressure losses are low as illustrated **Figure 8**.

The traditional analysis is majorly focused on evaluating the consequence of both process and geometric variables. However, in recent studies, the combined analysis of fiscal and process variables gained remarkable importance on the exergoeconomic performance [7, 24]. The primary reason is that the system operating with different economic variables i.e., interest rate, electricity cost, and intake

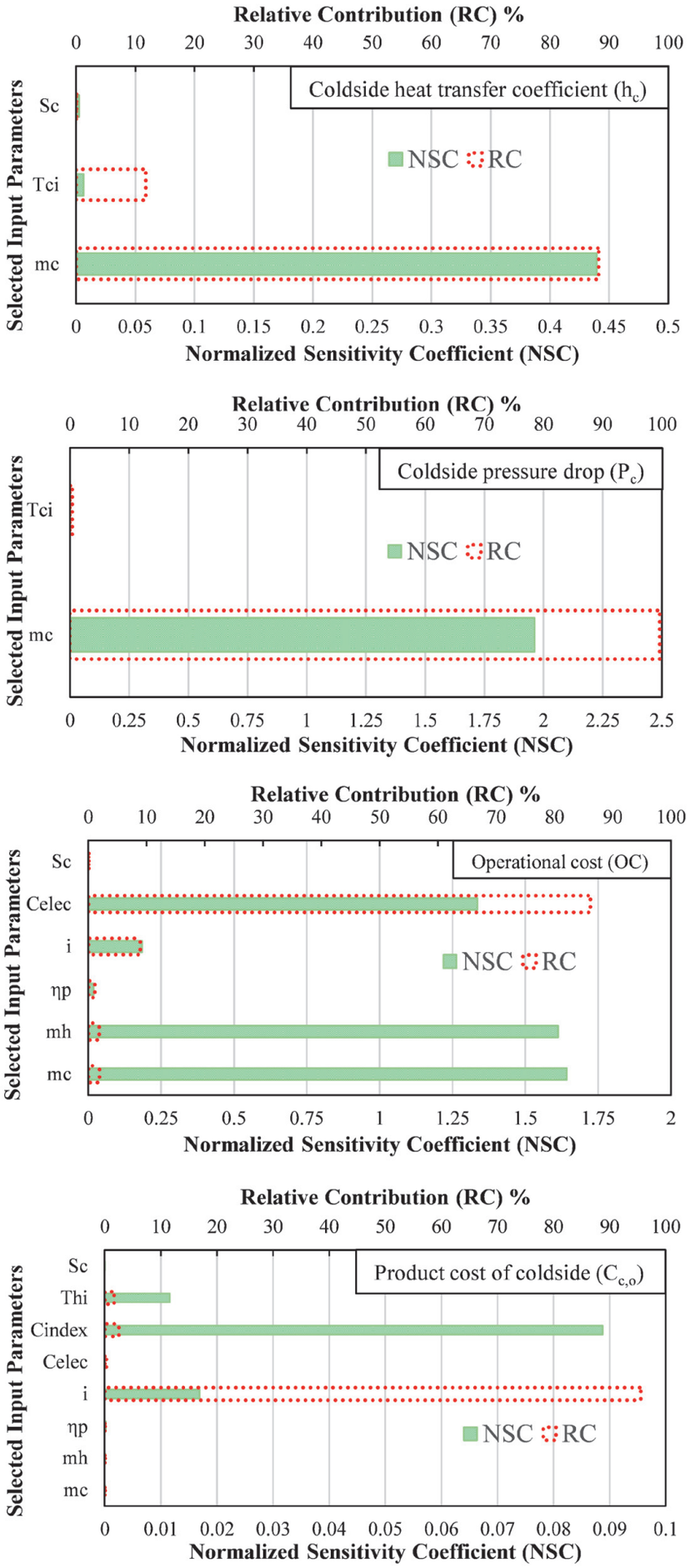

Figure 6.
Normalized Sensitivity analysis results for performance parameters of (a) heat transfer coefficient (h_c) (b) pressure drop (ΔP_c) (c) operational cost (OC) (d) product Cost ($C_{c,o}$).

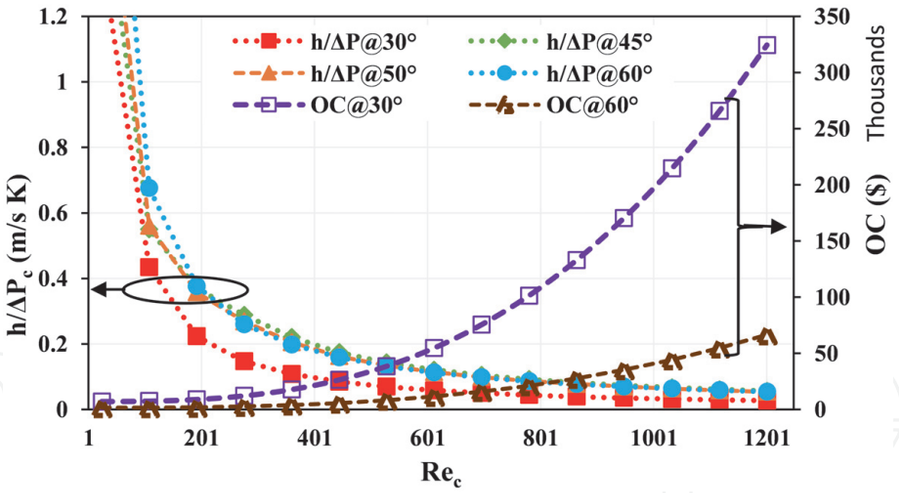

Figure 7.
Effect of Reynold number on heat transfer per unit pressure drop (h/ΔP) and operational cost (OC).

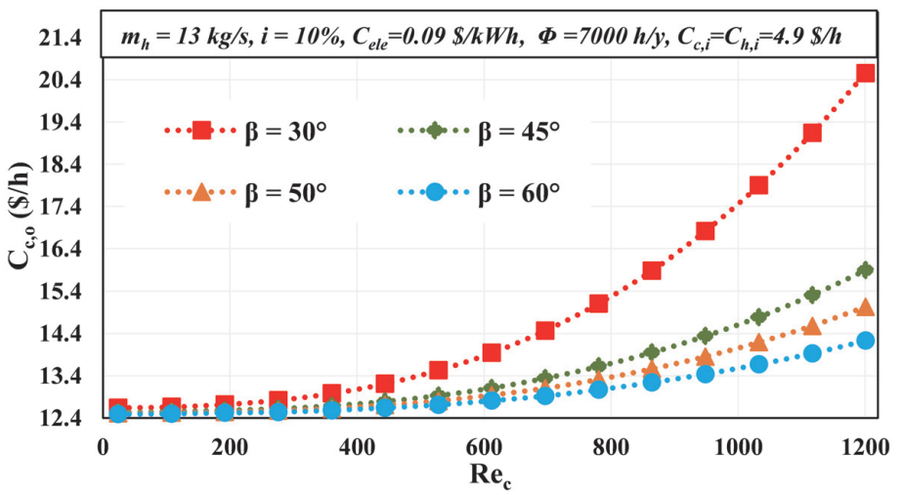

Figure 8.
Effect of Reynold number rate on the outlet cold stream cost ($\dot{C}_{c,o}$).

chemical cost would have different operation cost (OC) with like thermal and hydraulic performance [6, 18].

Therefore, an economic analysis is conducted for various economic policies over time as the importance of fiscal parameters is observed on performance parameters by sensitivity analysis as well in the above section. The cold stream product cost $C_{c,o}$ increased by varying the interest rate and electricity cost, as illustrated in **Figure 9a** and **b**. For example, by varying the inflate rate and from 1 to 14%, the $C_{c,o}$ increased ~17.7% for chevron angle β = 30°. Likewise, for the same chevron angle, the product cost $C_{c,o}$ increased ~3.80% by varying the electricity cost from 0.01 to 0.15 $/kWh. Furthermore, the outlet cost of the cold stream is highest for the β = 30° and lowest for the β = 60° for both interest rate and electricity cost.

An exergoeconomic flow diagram is a noteworthy pictorial demonstration of the thermo-economics output at every significant position of the system. It presents the economics and exergy of all streams at important points, i.e., inlet and outlets of each section of the large system. The visual representation is very substantial for the system with the multiple components to recognize how efficiently the induvial components are working from an economic and exergetic point of view. For the current case study, **Figure 10** demonstrates the exergoeconomic flow diagram.

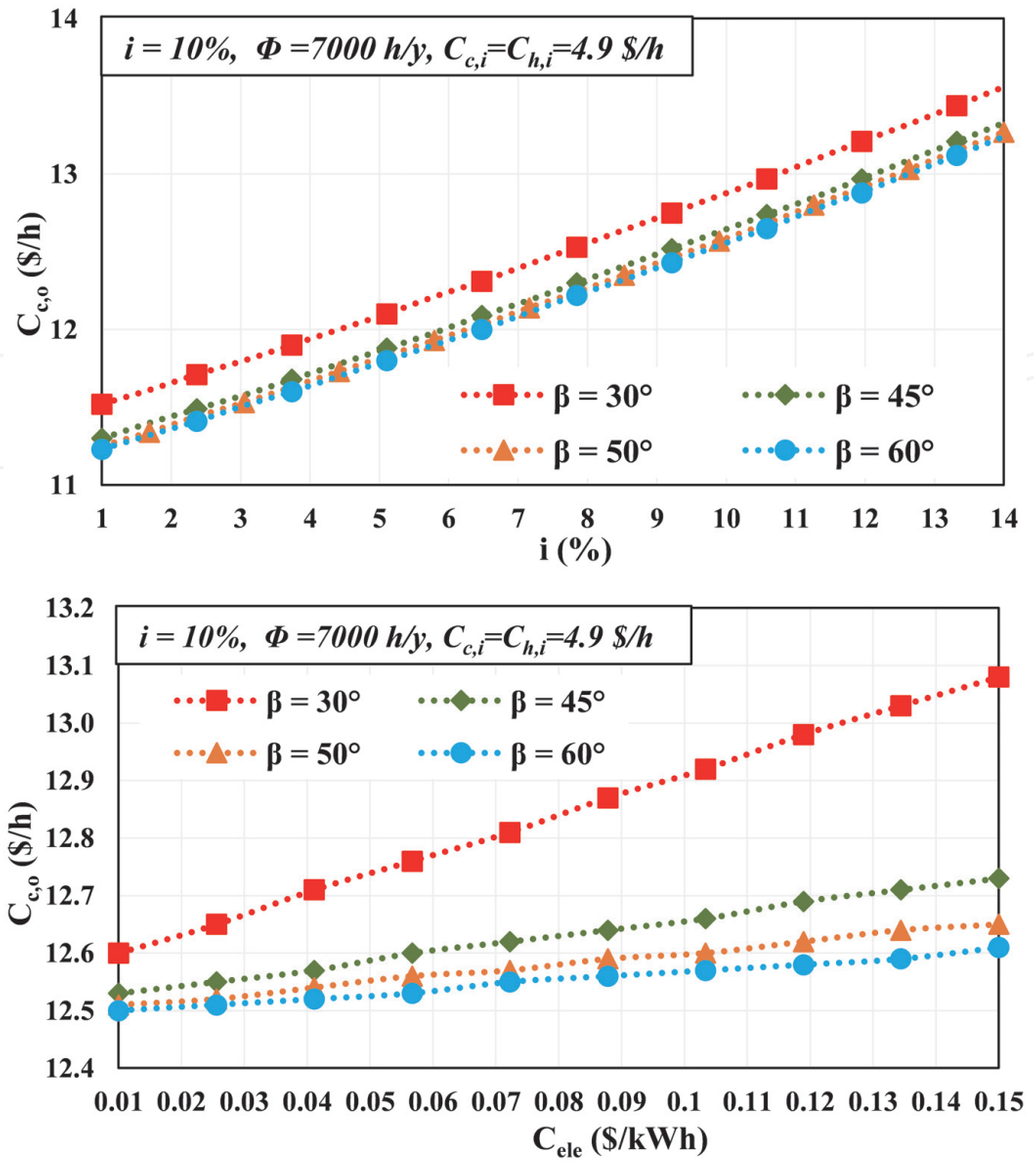

Figure 9.
Effect of monetary (a) cold water product cost ($\dot{C}_{c,o}$) against inflation rate, and (b) cold water product cost ($\dot{C}_{c,o}$) against electricity cost.

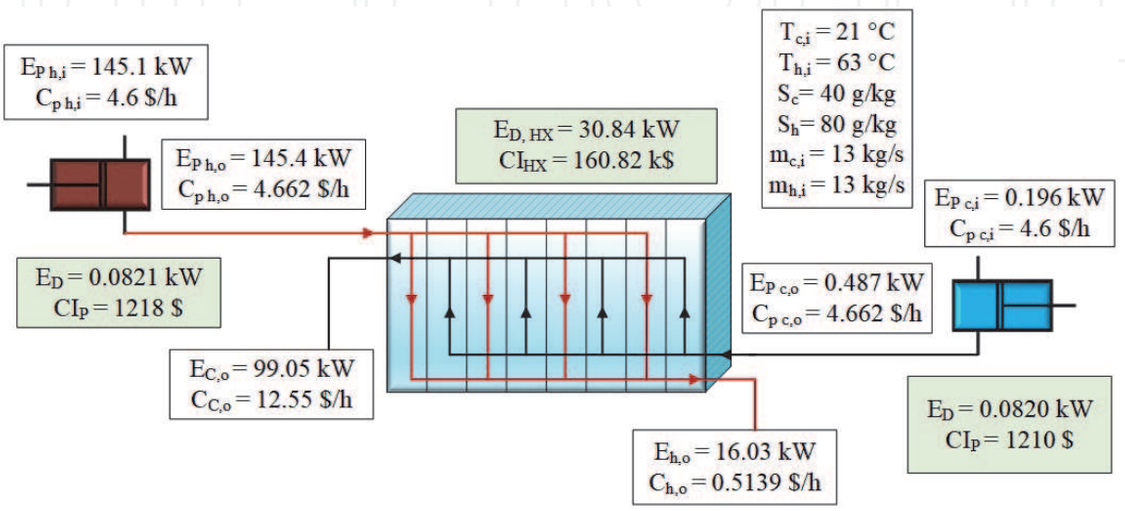

Figure 10.
Exergy-cost flow diagram for current PHX arrangement.

5. Concluding remarks

A corrugated plate heat exchanger (PHX) is examined as a preheater in SEE-MVC based-thermal desalination system to preheat the intake feedwater using the hot waste brine stream. The system is examined from the thermal, hydraulics, and economics point of view. For the case study, the EES-based numerical code is developed using governing equations. After that, the experimental data is used to validate the developed numerical model. Furthermore, sensitivity analysis is conducted in form of NSC and RC to classify the influential input variables. After that, the one-factor-at-a-time (OFAT) technique is used for the detailed parametric analysis to recognize the effect of influential variables. In the end, the exergoeconomic flow diagram is demonstrated to compute the exergies and product cost of the stream at each component of the system. The output of the current case study is as follows.

- The sensitivity analysis highlights that the utmost critical input variables in form of NSC are cold water mass flow rate followed by cold water inlet temperature, and salinity for the local cold water heat transfer coefficient. Similarly, the most critical parameters for the cold side pressure drop are the cold-water mass flow rate followed by the cold-water inlet temperature. Furthermore, the operation cost (OC), the most critical input variable are mass flow of cold water > mass flow of hot water > electricity cost > interest rate > and efficiency of the pump while the cold water outlet cost, the critical variables are cost index > inflation rate > inlet temperature of hot > efficiency of the pump > mass flow rate of water > mass flow rate of hot water >unit cost of electricity.

- The parametric analysis reflects that the comprehensive parameter ($h/\Delta P$) is decreased with an increase of Reynold number due to higher-order increment in pressure drop. Likewise, the operational cost (OC) and cold stream of outlet cost are increased because at high Reynold number, the pressure losses are increased which consume more energy and ultimately increase the pumping power to maintain the desired pressure and overcome the losses. The OC and cold fluid outlet cost is highest for the $\beta = 30°$ and lowermost for $\beta = 60°$ because at a high chevron angle, the pressure loss is low.

- The cold stream outlet cost increased by ~17.7% and ~3.80% by increased the inflation rate and unit cost of electricity respectively for the $\beta = 30°$.

Acknowledgements

The authors would like to thank KAUST Saudi Arabia and Northumbria University UK under reference # RDF20/EE/MCE/SHAHZAD for funding this research.

Conflict of interest

The authors declare no known conflict of interest.

Abbreviations

CI	capital investment
CEPCI	chemical engineering plant cost index
FOC	factor of cleanliness
EF	enlargement factor
HX	heat exchange
IF	installation factor
LMTD	log mean temperature difference
MED	multi-effect desalination
MSF	multistage flash
MVC	mechanical vapor compression
NSC	normalized sensitivity coefficients
PHXs	plate heat exchangers
OSD	over surface design
OFAT	one-factor-at-a-time
OC	running/operational cost
RC	relative contribution
TVC	thermal vapor compression

Nomenclature

A	heat transfer area, m^2
A_e	effective area, m^2
A_p	projected plate area, m^2
A_{sp}	single plate area, m^2
B	mean channel width, m
C_h	constant parameter for calculation of Nusselt number in Eq. (1)
$\dot{C}$	Outlet/product cost, ($/h)
C_{total}	total equipment cost, $
C_y	yearly current cost, $/y
C_{ele}	Electricity cost, $/kWh
C_{index}	cost index factor
D_p	diameter of port, m
D_{hyd}	hydraulic diameter, m
$\overline{EX}$	specific exergy, k.J/kg
ff	friction factor for pressure drop calculation
ν_{chl}	mass velocity per channel, kg/m^2s
h	heat transfer coefficient (local), W/m2K
h'	enthalpy, kJ
i	inflation/interest rate, %
k	thermal conductivity, W/mK
K_P	constant variable for friction factor calculation in **Table 3**
L_c	compressed plate length, m
L_h	length of horizontal port, m
L_p	vertical port distance from between port ends, m
L_v	vertical port distance between port centers, m
L_w	effective channel width, m
$\dot{m}$	mass flow rate, kg/s
Nu	Nusselt number
n_y	equipment life, year

N_e	effective number of plates
N_p	number of flow passes
N_{tb}	number of HX plates
N_{cpp}	number of flow channels per pass
PP	plate pitch, m
P_{Power}	pumping power, W
ΔP	pressure drop, Pa
Pr	Prandtl number
r	capital recovery factor
Re	Reynolds number
$R_{fo,\ total}$	total fouling resistance, m^2 K/W
S	salinity, g/kg
s	entropy, J/K
T	temperature, °C
t_{plate}	thickness of plate, m
U	global/overall heat transfer coefficient, W/m^2K
V	velocity of fluid, m/s
v_s	specific volume, m^3/kg
$\dot{W}_p$	work of pump, kW
$\dot{E}$	exergy flow rate, kW
$\dot{E}_D$	total exergy destruction, kW
$\dot{\Gamma}$	yearly capital investment rate, $/y

Greek Symbols

ς	rate of fixed cost, $/s
β	chevron angle, deg.
Δ	variation in magnitude
∂	partial
ρ	density, kg/m^3
μ	viscosity, kg/ms
Φ	plant availability/operating hours, hour/year
η_p	Pump efficiency

Subscripts

0	dead state
B	brine
c	cold water
cl	clean
c,i	cold inlet
c,o	cold outlet
chl	per channel
fo	fouled
h	hot
h,i	hot inlet
h,o	hot outlet
i	in
man	manifold
o	out

p	pump
po	port
SW	Seawater
tot	total
w	wall

Superscripts

m	constant parameter for calculation of friction factor in **Table 3**
n	constant parameter for calculation of Nusselt number in Eq. (1)
w	wall

Author details

Muhammad Ahmad Jamil[1*], Talha S. Goraya[2], Haseeb Yaqoob[2], Kim Choon Ng[3], Muhammad Wakil Shahzad[1] and Syed M. Zubair[4]

1 Department of Mechanical and Construction Engineering, Northumbria University, Newcastle Upon Tyne, United Kingdom

2 Department of Mechanical Engineering, Khwaja Fareed University of Engineering and Information Technology, Rahim Yar Khan, Pakistan

3 Water Desalination and Reuse Center, King Abdullah University of Science and Technology, Thuwal, Saudi Arabia

4 Department of Mechanical Engineering, King Fahd University of Petroleum and Minerals, Dhahran, Saudi Arabia

*Address all correspondence to: muhammad2.ahmad@northumbria.ac.uk

References

[1] Abid, A.; Jamil, M. A.; Sabah, N. us; Farooq, M. U.; Yaqoob, H.; Khan, L. A.; Shahzad, M. W. Exergoeconomic Optimization of a Forward Feed Multi-Effect Desalination System with and without Energy Recovery. Desalination, 2020, 499 (July 2020), 114808. DOI: 10.1016/j.desal.2020.114808.

[2] Shahzad MW, Burhan M, Ybyraiymkul D, Ng KC. Desalination processes' efficiency and future roadmap. Entropy. 2019;**21**(1):84. DOI: 10.3390/e21010084

[3] Jamil, M. A.; Shahzad, M. W.; Zubair, S. M. A Comprehensive framework for Thermoeconomic analysis of desalination systems. Energy Convers. Manag., 2020, 222 (June), 113188. DOI:10.1016/j.enconman.2020.113188.

[4] Chitgar N, Emadi MA, Chitsaz A, Rosen MA. Investigation of a novel multigeneration system driven by a SOFC for electricity and fresh water production. Energy Convers. Manag. 2019;**196**(June):296-310. DOI: 10.1016/j.enconman.2019.06.006.

[5] Elsayed ML, Mesalhy O, Mohammed RH, Chow L. C. Transient Performance of MED Processes with Di Ff Erent Feed Con Fi Gurations. 2018; **438**(March):37-53. DOI: 10.1016/j.desal.2018.03.016

[6] Jamil MA, Zubair SM. Effect of feed flow arrangement and number of evaporators on the performance of multi-effect mechanical vapor compression desalination systems. Desalination. September 2017; **2018**(429):76-87. DOI: 10.1016/j.desal.2017.12.007

[7] Jamil MA, Zubair SM. Design and analysis of a forward feed multi-effect mechanical vapor compression desalination system: An Exergo-economic approach. Energy. 2017;**140**: 1107-1120. DOI: 10.1016/j.energy.2017.08.053

[8] Zhou Y, Shi C, Dong G. Analysis of a mechanical vapor recompression wastewater distillation system. Desalination. 2014;**353**:91-97. DOI: 10.1016/j.desal.2014.09.013

[9] Ettouney H. Design of Single-Effect Mechanical Vapor Compression. Desalination. 2006;**190**:1-15. DOI: 10.1016/j.desal.2005.08.003

[10] Elsayed ML, Mesalhy O, Mohammed RH, Chow LC. Transient performance of MED processes with different feed configurations. Desalination. December 2017; **2018**(438):37-53. DOI: 10.1016/j.desal.2018.03.016

[11] Ettouney HM, El-Dessouky HT. Fundamentals of salt water. Desalination. 2002

[12] Abdelkader BA, Jamil MA, Zubair SM. Thermal-hydraulic characteristics of helical baffle Shell-and-tube heat exchangers. Heat Transf. Eng. 2019. DOI: 10.1080/01457632.2019.1611135

[13] Nilpueng K, Keawkamrop T, Ahn HS, Wongwises S. Effect of Chevron angle and surface roughness on thermal performance of single-phase water flow inside a plate heat exchanger. Int. Commun. Heat Mass Transf. 2018;**91**:201-209. DOI: 10.1016/j.icheatmasstransfer.2017.12.009

[14] Shon BH, Jung CW, Kwon OJ, Choi CK, Kang YT. Characteristics on condensation heat transfer and pressure drop for a low GWP refrigerant in brazed plate heat exchanger. Int. J. Heat Mass Transf. 2018;**122**:1272-1282. DOI: 10.1016/j.ijheatmasstransfer.2018.02.077.

[15] Hajabdollahi F, Hajabdollahi Z, Hajabdollahi H. Optimum Design of Gasket Plate Heat Exchanger Using Multimodal Genetic Algorithm. Heat Transf. Res. 2013;**44**(8):761-789. DOI: 10.1615/HeatTransRes.2013006366

[16] Hajabdollahi H, Naderi M, Adimi S. A comparative study on the Shell and tube and gasket-plate heat exchangers: The economic viewpoint. Appl. Therm. Eng. 2016;**92**:271-282. DOI: 10.1016/j.applthermaleng.2015.08.110

[17] Jamil MA, Din ZU, Goraya TS, Yaqoob H, Zubair SM. Thermal-hydraulic characteristics of Gasketed plate heat exchangers as a preheater for thermal desalination systems. Energy Convers. Manag. 2020;**205**(October 2019):112425. DOI: 10.1016/j.enconman.2019.112425

[18] Jamil MA, Zubair SM. On Thermoeconomic analysis of a single-effect mechanical vapor compression desalination system. Desalination. 2017; **420**(July):292-307. DOI: 10.1016/j.desal.2017.07.024.

[19] Kakac S, Liu HHE. Selection, Rating, and Thermal Design. 2nd ed. New York: CRC; 2002

[20] Khairul MA, Alim MA, Mahbubul IM, Saidur R, Hepbasli A, Hossain A. Heat transfer performance and exergy analyses of a corrugated plate heat exchanger using metal oxide Nanofluids. Int. Commun. Heat Mass Transf. 2014;**50**:8-14. DOI: 10.1016/j.icheatmasstransfer.2013.11.006

[21] Mistry KH, McGovern RK, Thiel GP, Summers EK, Zubair SM, Lienhard V, et al. Analysis of desalination technologies. Entropy. 2011;**13**(12):1829-1864. DOI: 10.3390/e13101829.

[22] Nayar KG, Sharqawy MH, Banchik LD, Lienhard V. J. H. Thermophysical properties of seawater: A review and new correlations that include pressure dependence. Desalination. 2016;**390**:1-24. DOI: 10.1016/j.desal.2016.02.024.

[23] Sadeghzadeh H, Ehyaei MA, Rosen MA. Techno-economic optimization of a Shell and tube heat exchanger by genetic and particle swarm algorithms. Energy Convers. Manag. 2015;**93**:84-91. DOI: 10.1016/j.enconman.2015.01.007

[24] Jamil MA, Elmutasim SM, Zubair SM. Exergo-economic analysis of a hybrid humidification dehumidification reverse osmosis (HDH-RO) system operating under different retrofits. Energy Convers. Manag. September 2017;**2018**(158): 286-297. DOI: 10.1016/j.enconman.2017.11.025

[25] Caputo AC, Pelagagge PM, Salini P. Heat exchanger design based on economic optimisation. Appl. Therm. Eng. 2008;**28**(10):1151-1159. DOI: 10.1016/j.applthermaleng.2007.08.010

[26] El-Sayed YM. The Thermoeconomics of Energy Conversions. Amsterdam: Elsevier; 2003

[27] El-Mudir W, El-Bousiffi M, Al-Hengari S. Performance evaluation of a small size TVC desalination plant. Desalination. 2004;**165**:269-279

[28] El-Sayed YM. Designing desalination Systems for Higher Productivity. Desalination. 2001;**134**(1–3):129-158. DOI: 10.1016/S0011-9164(01)00122-9

[29] Jamil MA, Goraya TS, Ng KC, Zubair SM, Bin B, Shahzad MW. Optimizing the energy recovery section in thermal desalination Systems for Improved Thermodynamic, economic, and environmental performance. Int. Commun. Heat Mass Transf. 2021;**124**: 105244. DOI: 10.1016/j.icheatmasstransfer.2021.105244

[30] Zhang C, Liu C, Wang S, Xu X, Li Q. Thermo-economic comparison of subcritical organic Rankine cycle based on different heat exchanger configurations. Energy. 2017;**123**: 728-741. DOI: 10.1016/j.energy.2017.01.132

[31] Li J, Yang Z, Hu S, Yang F, Duan Y. Effects of Shell-and-tube heat exchanger arranged forms on the thermo-economic performance of organic Rankine cycle systems using hydrocarbons. Energy Convers. Manag. 2020;**203**(October 2019):112248. DOI: 10.1016/j.enconman.2019.112248

[32] Vatavuk WM. Updating the CE plant cost index. Chem. Eng. 2002;**1** (January):62-70

[33] Jenkins, S. 2019 Chemical engineering plant cost index annual average https://www.chemengonline.com/2019-chemical-engineering-plant-cost-index-annual-average/ (accessed Apr 9, 2020).

[34] Jamil, M. A.; Xu, B. Bin; Dala, L.; Sultan, M.; Jie, L.; Shahzad, M. W. Experimental and Normalized Sensitivity Based Numerical Analyses of a Novel Humidifier-Assisted Highly Efficient Indirect Evaporative Cooler. Int. Commun. Heat Mass Transf., 2021, 125, 105327. DOI:10.1016/j.icheatmasstransfer.2021.105327.

[35] Jamil, M. A.; Goraya, T. S.; Shahzad, M. W.; Zubair, S. M. Exergoeconomic optimization of a Shell-and-tube heat exchanger. Energy Convers. Manag., 2020, 226 (September), 113462. DOI: 10.1016/j.enconman.2020.113462.

[36] James CA, Taylor RP, Hodge BK. The application of uncertainty analysis to cross-flow heat exchanger performance predictions. Heat Transf. Eng. 1995;**16**(4):50-62. DOI: 10.1080/01457639508939863.